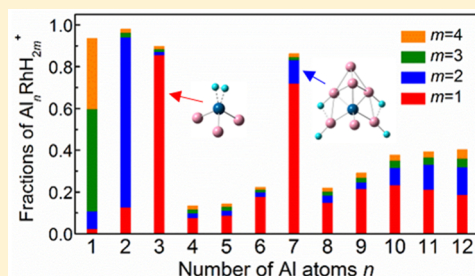


Size Dependent H₂ Adsorption on Al_nRh⁺ (*n* = 1–12) ClustersMeiye Jia,[†] Jan Vanbuel,[†] Piero Ferrari,[†] Eva M. Fernández,[‡] Sandy Gewinner,[§] Wieland Schöllkopf,[§] Minh Tho Nguyen,^{||} André Fielicke,[§] and Ewald Janssens^{*,†}[†]Laboratory of Solid State Physics and Magnetism, KU Leuven, Celestijnenlaan 200D, 3001 Leuven, Belgium[‡]Departamento de Física Fundamental, UNED, Paseo Senda del Rey 9, 28040 Madrid, Spain[§]Fritz-Haber-Institut der Max-Planck-Gesellschaft, Faradayweg 4–6, 14195 Berlin, Germany^{||}Department of Chemistry, KU Leuven, Celestijnenlaan 200F, 3001 Leuven, Belgium

Supporting Information

ABSTRACT: The interaction of hydrogen with singly rhodium doped aluminum clusters Al_nRh⁺ (*n* = 1–12) is investigated experimentally by a combination of time-of-flight mass spectrometry and infrared multiple photon dissociation (IRMPD) spectroscopy. Density functional theory (DFT) is employed to optimize the geometric and electronic structures of bare and hydrogenated Al_nRh⁺ clusters and the obtained infrared spectra of hydrogenated clusters are compared with the corresponding IRMPD spectra. The reactivity of the Al_nRh⁺ clusters toward H₂ is found to be strongly size-dependent, with *n* = 1–3, and 7 being the most reactive. Furthermore, it is favorable for H₂ to adsorb molecularly on Al₂Rh⁺ and Al₃Rh⁺, while it prefers dissociative adsorption on other sizes. The initial molecular adsorption of H₂ is identified as the determining step for hydrogen interaction with the Al_nRh⁺ clusters, because the calculated molecular adsorption energies of H₂ correlate well with the experimental abundances of the hydrogenated clusters. Natural charge populations and properties of the Al_nRh⁺ clusters are analyzed to interpret the observed size-dependent reactivity.



1. INTRODUCTION

Hydrogen (H₂) has a great potential as energy carrier in sustainable energy systems because of its environmental friendliness, high efficiency, and low cost.^{1,2} However, the employment of hydrogen for our daily energy supply is so far limited; one of the main issues is the storage of hydrogen. Current applications make use of hydrogen as compressed gas or in the liquid form, both having an energy density that is much lower than that of gasoline.³ Solid-state hydrogen storage is potentially superior with respect to storage capacity, energy efficiency, and safety.⁴ One of these solid-state storage strategies is to store the hydrogen chemically in the form of metal hydrides.^{5–7} Aluminum-based alloys are one group of promising hydrogen storage materials due to their low weight, low cost, and high storage capacity.⁷ It has been acknowledged that atomic clusters can be considered as model systems to study the active sites of pure metal and alloy surfaces.⁸ In this respect, the investigation of H₂ interacting with metal clusters under well-controlled conditions can contribute to elucidate molecular level mechanisms for metal hydrogenation involved in hydrogen storage.⁹

Pure aluminum clusters, except Al_{6,7}^{0/+}, do not adsorb hydrogen as is the case for bulk aluminum. Computational studies suggest that the low reactivity of aluminum clusters toward H₂ is due to kinetic impediment of the hydrogenation reaction by a high activation barrier.¹⁰ Experimentally, the chemisorption of H₂ on neutral bimetallic clusters Co_nAl_m and Nb_nAl_m was studied in a fast flow reactor in combination with

mass spectrometry and the observed composition dependent reactivity was attributed to geometric and charge transfer effects.¹¹ In addition, H₂ interaction with transition metal doped aluminum clusters has been investigated computationally for MAI_n (M = Mg, Ca, Sc, Y, Ti, V, Cr, Zr, Nb, etc.).^{12–15} These studies enhanced the fundamental insights into the mechanisms of H₂ adsorption, activation, and dissociation as well as the role of dopant atoms during these processes.

Rhodium has a high affinity toward hydrogen absorption and forms metal hydrides.¹⁶ It is useful for hydrogen storage applications due to its excellent hydrogen solubility and diffusivity.^{16–18} H₂ adsorption and dissociation on Mg_nRh (*n* = 1–10) has been studied computationally.¹⁹ It was found that Rh doping significantly reduces the activation barriers for hydrogen dissociation, which are present in bare Mg_n clusters. Recently, H₂ adsorption on single vanadium(V) and doubly rhodium (Rh) doped aluminum clusters was investigated by time-of-flight mass spectrometry and infrared multiple photon dissociation spectroscopy (IRMPD) combined with density functional theory (DFT) calculations.^{20,21} Both dopants were shown to enhance the reactivity of aluminum clusters toward hydrogen in a size-dependent way. DFT calculations underlined the importance of activation barriers in the chemisorption process for the smaller Al_nV⁺ (*n* = 2–8, and 10)

Received: May 7, 2018

Revised: July 23, 2018

Published: July 23, 2018

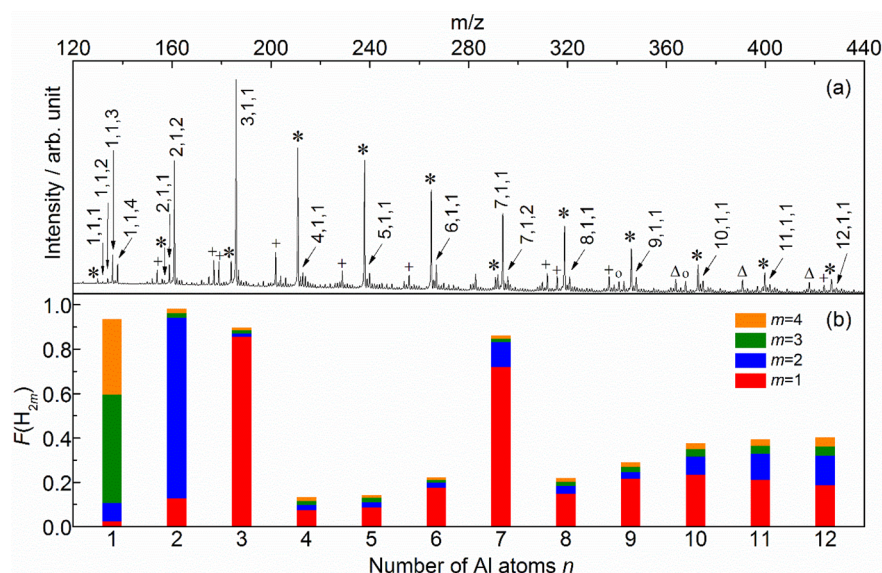


Figure 1. (a) Mass spectrum of hydrogenated Al_nRh^+ ($n = 1-12$) clusters and (b) fractions of $\text{Al}_n\text{RhH}_{2m}^+$ ($n = 1-12$, $m = 1-4$) clusters. The labels n,l,m in (a) indicate $\text{Al}_n\text{RhH}_{2m}^+$. Peaks labeled with an asterisk (*) correspond to bare Al_nRh^+ ($n = 1-12$) clusters. Additional signals labeled with the symbols \circ , Δ , and $+$ can be assigned to $\text{Al}_{5-6}\text{Rh}_2^+$, $\text{Al}_{2-4}\text{Rh}_3^+$, and metal hydroxides of Al_nRh_x^+ , respectively.

clusters. Orbital analysis showed that the activation barriers are due to an unfavorable overlap between cluster and hydrogen orbitals.²⁰ For H_2 adsorption on Al_nRh_2^+ ($n = 10-13$) clusters,²¹ it was concluded that a single H_2 molecule binds dissociatively for $n = 10$ and 11 , whereas it adsorbs molecularly for $n = 12$ and 13 . DFT calculations suggest that the molecular adsorption for $n = 12$ and 13 is due to a high binding energy between H_2 and the clusters and not a consequence of kinetic impediment of the hydrogenation reaction by an activation barrier. The hydrogen molecule initially forms a strongly bound Kubas complex with the $\text{Al}_{11-13}\text{Rh}_2^+$ clusters, whereas it binds only weakly with $\text{Al}_{10}\text{Rh}_2^+$.

In this paper, the interaction of H_2 with a series of Al_nRh^+ ($n = 1-12$) clusters is investigated by DFT calculations in combination with mass spectrometry and IRMPD spectroscopy. We are exploring the size dependent reactivity of Al_nRh^+ clusters toward H_2 , aiming to shed light on the design and selection of potential rhodium–aluminum alloys for hydrogen storage.

2. EXPERIMENTAL AND THEORETICAL METHODS

2.1. Experimental Methods. The Al_nRh^+ ($n = 1-12$) clusters are produced in a dual laser ablation source.²² In short, the second harmonic light of two Nd:YAG lasers ($\lambda = 532$ nm) is focused onto rotating Al and Rh rods to create a hot plasma. A short pulse of helium (He) carrier gas with a backing pressure of 5 bar serves to cool down the plasma. The clusters are formed and thermalized by the carrier gas in the source, which is kept at room temperature. Hydrogen gas at a backing pressure of 1 bar is injected through a separate valve, located close to the nozzle of the source. By careful selection of the timing sequence, dissociation of molecular hydrogen in the ablation plasma is avoided. Expansion from the high-pressure region of the source into the vacuum generates a beam of metal clusters and cluster-hydrogen complexes. A 2 mm skimmer is used to select the central part of this molecular beam containing both neutral and charged particles. The cationic particles are extracted into an orthogonal time-of-flight mass spectrometer for abundance analysis. IRMPD spectra are

obtained by scanning the light of the free-electron laser (FEL) of the Fritz-Haber-Institut der Max-Planck-Gesellschaft²³ in the range of $800-2100$ cm^{-1} (~ 50 mJ in a ~ 10 μs long pulse, $5-10$ cm^{-1} FWHM bandwidth) and focusing it onto a 1 mm aperture through which the cations pass before entering the extraction zone of the mass spectrometer. When the infrared light is in resonance with one of the IR active vibrational modes of the cluster-hydrogen complexes, one or multiple photons can be absorbed, thereby heating up the cluster through internal vibrational redistribution.²⁴ If several photons are adsorbed, the internal energy can reach the dissociation limit and the abundance of the corresponding $\text{Al}_n\text{RhH}_{2m}^+$ species in the mass spectrum will deplete.²¹ The IRMPD cross section σ of a cluster at a specific wavelength ν can be calculated as

$$\sigma(\nu) = -\frac{\log\left(\frac{I}{I_0}\right)}{P(\nu)} \quad (1)$$

in which I and I_0 are the abundances of the hydrogenated complex in the mass spectrum with and without FEL, and $P(\nu)$ is the energy per pulse at that wavelength. A complicating factor in the analysis of the IRMPD spectrum is the possibility of competing ingrowths and depletions when multiple hydrogen molecules are adsorbed onto one cluster. However, except for AlRh^+ and AlRh_2^+ , the abundances of the clusters with one hydrogen molecule is much larger than those with multiple H_2 molecules. Thus, the effect of competing channels on the depletion spectra is limited.

2.2. Computational Methods. DFT calculations are performed by employing the Gaussian 09 software package²⁵ with the generalized gradient approximated (GGA) exchange correlation functional as devised by Perdew–Burke–Ernzerhof (PBE).²⁶ This functional was previously adopted in our work for H_2 adsorption on double rhodium doped clusters, Al_nRh_2^+ ($n = 10-13$).²¹ PBE was also shown to perform well for structure determinations of several cationic binuclear transition-metal complexes²⁷ as well as interpretation of the

adsorption and dissociation behavior of NO molecules on small Rh_n^\pm clusters.²⁸

Global optimizations were carried out for Al_nRh^+ ($n = 1-12$) clusters and their hydrogenated counterparts $\text{Al}_n\text{RhH}_{2m}^+$ ($n = 1-3$, $m = 1-4$ and $n = 4-12$, $m = 1-2$) by the CALYPSO methodology.^{29,30} The low-lying isomers were collected and optimized for a range of possible spin multiplicities with the Stuttgart/Dresden (SDD) basis set³¹ and the corresponding effective core potential (ECP) for Rh and the TZVP basis set³² for Al and H. For each size, several low-lying energy isomers were further optimized by using the Def2TZVP basis set³³ for all the atoms. In addition to searching by CALYPSO, we manually built various initial structures for Al_nRh^+ clusters based on pure rhodium and aluminum counterparts. For $\text{Al}_n\text{RhH}_2^+$, a large number of structures were constructed and tested by adding two H atoms or one H_2 molecule to the low-lying isomers of Al_nRh^+ . Various orientations have been considered for the bonded H atoms (terminal, bridging, and facet sites) and H_2 molecule (end-on and side-on). At the PBE/Def2TZVP level, harmonic and anharmonic vibrational frequency calculations were performed to simulate the IR spectra and to obtain the zero-point energy (ZPE) corrections for the electronic energies. The vibrational frequencies are unscaled. To calculate H_2 adsorption energies, at the PBE/Def2TZVP level, we employed the D3 version of Grimme's dispersion corrections with Becke–Johnson damping (GD3BJ).

3. RESULTS

3.1. Mass Spectra. A typical mass spectrum of hydrogenated Al_nRh^+ ($n = 1-12$) clusters is shown in Figure 1a. Hydrogenated products, $\text{Al}_n\text{RhH}_{2m}^+$ ($n = 1-12$, $m = 1-4$), are seen at equidistant spacing of two mass units after the bare clusters. For AlRh^+ , the most abundant hydrogenated species is AlRhH_6^+ , while for Al_2Rh^+ the most intense one is $\text{Al}_2\text{RhH}_4^+$. For other sizes ($n = 3-12$), $\text{Al}_n\text{RhH}_2^+$ products predominate the observed hydrogenated clusters. Figure 1b shows the fractions of $\text{Al}_n\text{RhH}_{2m}^+$ ($n = 1-12$, $m = 1-4$), which are obtained by using the peak intensities (I) from the mass spectrum:

$$[F(\text{H}_{2m})] = \frac{I(\text{Al}_n\text{RhH}_{2m}^+)}{\sum_{i=0}^4 I(\text{Al}_n\text{RhH}_{2i}^+)} \quad (2)$$

Those fractions provide a qualitative means to assess the reactivity of Al_nRh^+ ($n = 1-12$) clusters toward H_2 . Apparently, the Al_nRh^+ clusters exhibit a strong size-dependent reactivity. Sizes $n = 1-3$ and 7 are most reactive, while particularly low reactivities are observed for $n = 4-6$ and 8. This distinct size dependence will be explained by complementary DFT calculations and discussed in section 4.

3.2. Structures of $\text{Al}_n\text{RhH}_{2m}^+$ ($n = 1-12$, $m = 0-2$) Clusters. Figure 2 shows the PBE/Def2TZVP optimized lowest energy structures for bare Al_nRh^+ ($n = 1-12$) clusters and hydrogenated $\text{Al}_n\text{RhH}_2^+$ and $\text{Al}_n\text{RhH}_4^+$ complexes. For single H_2 adsorption, both molecular ($\text{Al}_n\text{Rh}\cdot\text{H}_2^+$) and dissociative ($\text{Al}_n\text{RhH}_2^+$) configurations are included. A large number of isomers for Al_nRh^+ ($n = 1-12$), $\text{Al}_n\text{RhH}_{2m}^+$ ($n = 1-3$, $m = 1-4$), and $\text{Al}_n\text{RhH}_{2m}^+$ ($n = 4-12$, $m = 1-2$), calculated at the PBE/SDD&TZVP level, are shown in Figures S1–S8 in the Supporting Information (SI). The lowest energy structures are found to prefer the lowest possible spin states, i.e., singlet for the even electron systems ($n = 2, 4, 6, 8, 10,$

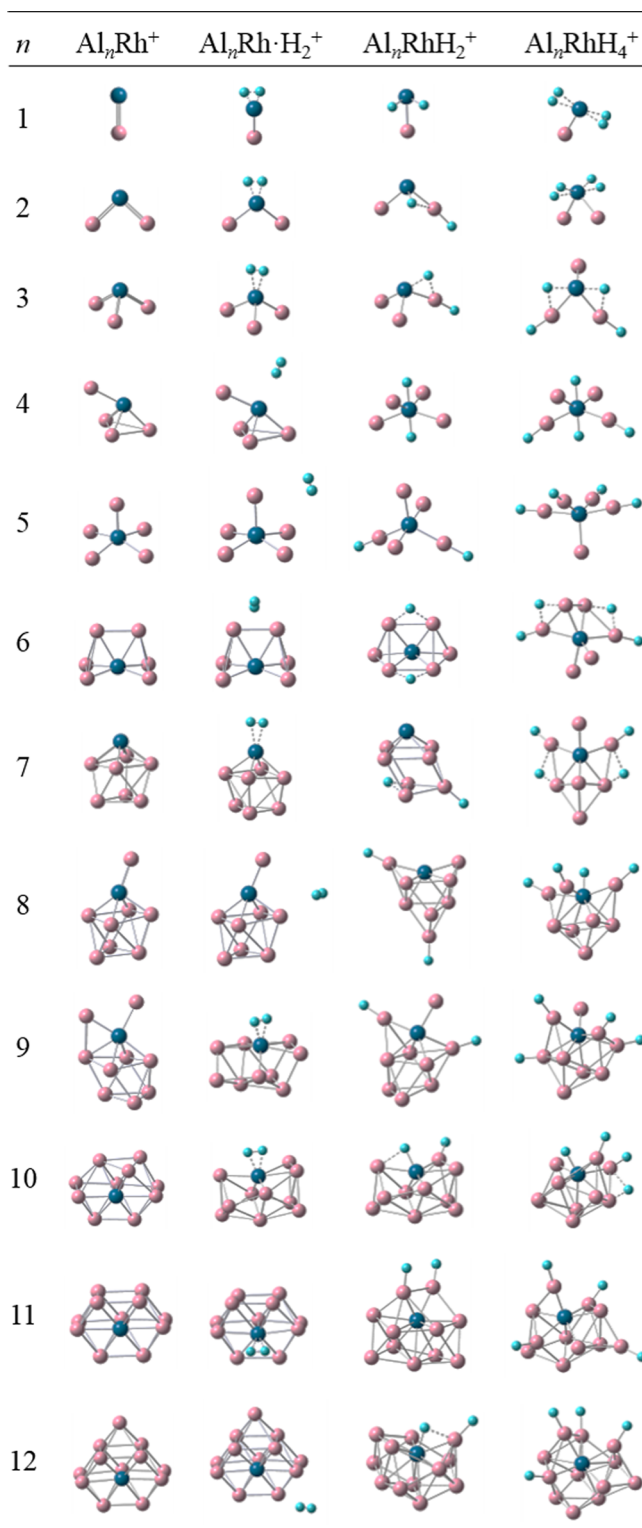


Figure 2. PBE/Def2TZVP optimized lowest energy structures for Al_nRh^+ , $\text{Al}_n\text{Rh}\cdot\text{H}_2^+$, $\text{Al}_n\text{RhH}_2^+$, and $\text{Al}_n\text{RhH}_4^+$ ($n = 1-12$). Blue, pink, and cyan spheres represent Rh, Al, and H atoms, respectively.

12) and doublet for the odd electron systems ($n = 1, 3, 5, 7, 9,$ and 11).

3.2.1. Bare Al_nRh^+ ($n = 1-12$) Clusters. For bare clusters, all equilibrium structures are three-dimensional except for the trivial cases with $n = 1$ and 2. As the number of Al atoms increases, the preferred position of the Rh atom changes from

top sites over convex capping sites to partially encapsulated sites within the aluminum frameworks. In Al_2Rh^+ and Al_3Rh^+ , each Al atom binds to Rh, without formation of Al–Al bonds. The cluster Al_4Rh^+ can be derived by adding one Al atom to the Rh atom in Al_3Rh^+ . For Al_5Rh^+ , each Al atom binds to the Rh atom without formation of an Al–Al bond. For Al_6Rh^+ , all of the Al atoms bind to the Rh atom with formation of several Al–Al bonds. In Al_7Rh^+ , the Rh atom is located at a capping position forming a distorted tetrahedral pyramid with four of the Al atoms while the remaining three Al atoms bind to this moiety by Al–Al bonds. Al_8Rh^+ and Al_9Rh^+ can be obtained by adding one or two Al atoms on top of the Rh atom in Al_7Rh^+ . The $\text{Al}_{10-12}\text{Rh}^+$ clusters have cage-like structures in which the Rh dopant is partially encapsulated by the framework formed by Al atoms.

3.2.2. Single H_2 Addition Complexes $\text{Al}_n\text{Rh}\cdot\text{H}_2^+$ and $\text{Al}_n\text{RhH}_2^+$ ($n = 1-12$). For molecular H_2 addition, $\text{Al}_n\text{Rh}\cdot\text{H}_2^+$, the H_2 molecule binds to the Rh atom for $n = 1-4, 7$, and $9-11$ while it adds to one of the Al atoms for sizes $n = 5, 6, 8$, and 12 . For dissociative H_2 adsorption, $\text{Al}_n\text{RhH}_2^+$, the preferred adsorption sites for the two H atoms depend on the cluster size. Both of the two H atoms are predicted to bind to the Rh atom for $n = 1$ and 4 . For $n = 2, 3, 10$, and 12 , one of the two H atoms binds to an Al atom, while the other one binds at a Rh–Al bridge position. For other sizes, the two H atoms bind on top of Al atoms ($n = 5, 8, 9$, and 11), both of the H atoms locate at Al–Al bridge sites ($n = 6$), or one H atom binds to top Al and the other one to an Al–Al bridge site ($n = 7$).

3.2.3. Double H_2 Addition Complexes $\text{Al}_n\text{RhH}_4^+$ ($n = 1-12$). For double H_2 adsorption, both H_2 molecules bind molecularly to the Rh atom for $n = 1$ and 2 , while they absorb dissociatively for other sizes ($n = 3-12$). For $\text{Al}_3\text{RhH}_4^+$, two of the four H atoms bind to terminal Al atoms and the other two bind at Rh–Al bridge positions. In $\text{Al}_4\text{RhH}_4^+$, two H atoms bind terminally to Al atoms and the other two to the Rh atom. For the sizes $n = 5-7, 9, 11$, and 12 , all of the four H atoms bind to Al atoms at terminal or bridging sites. For $n = 8$ and 10 , one of the four H atoms binds to the Rh atom and the others to Al atoms.

3.3. H_2 Adsorption on Al_nRh^+ ($n = 1-12$) Clusters.

Table 1 summarizes the calculated adsorption energies

Table 1. PBE(GD3BJ)/Def2TZVP Calculated Molecular, $-E_{\text{ads}}(\text{H}_2)/\text{eV}$, and Dissociative, $-E_{\text{ads}}(2\text{H})/\text{eV}$, Adsorption Energies (ZPE Corrections Are Included) for Single H_2 Adsorption on Al_nRh^+ ($n = 1-12$) Clusters^a

n	$-E_{\text{ads}}(\text{H}_2)/\text{eV}$	$-E_{\text{ads}}(2\text{H})/\text{eV}$	$d(\text{H}-\text{H})/\text{\AA}$	$d(\text{M}-\text{H}_2)/\text{\AA}$
1	0.93	1.10	0.95	1.64
2	0.84	0.77	0.88	1.72
3	0.47	0.20	0.82	1.84
4	0.06	0.94	0.76	2.38
5	0.03	1.11	0.75	3.18
6	0.05	1.31	0.76	2.87
7	0.31	0.63	0.80	1.91
8	0.03	0.86	0.75	3.07
9	0.19	1.02	0.86	1.78
10	0.29	1.09	0.99	1.69
11	0.24	0.67	0.91	1.74
12	0.03	0.96	0.76	2.86

^aThe H–H bond lengths $d(\text{H}-\text{H})/\text{\AA}$ and M– H_2 distances $d(\text{M}-\text{H}_2)/\text{\AA}$ in the case of molecular adsorption are given.

$-E_{\text{ads}}(\text{H}_2)$ and $-E_{\text{ads}}(2\text{H})$ for molecular ($\text{Al}_n\text{Rh}\cdot\text{H}_2^+$) and dissociative ($\text{Al}_n\text{RhH}_2^+$) single H_2 adsorption on free Al_nRh^+ ($n = 1-12$) clusters. In addition, the H–H bond lengths, $d(\text{H}-\text{H})$, and M– H_2 distances, $d(\text{M}-\text{H}_2)$ (M = Al or Rh depending on the H_2 adsorption site), in the case of molecular H_2 adsorption are included.

Both the molecular and dissociative H_2 adsorption on Al_nRh^+ clusters are exothermic, though the molecular adsorption energies are smaller for $n = 4-6, 8$, and 12 . The $-E_{\text{ads}}(\text{H}_2)$ range from 0.03 to 0.93 eV and maxima are for $n = 1-3$ and 7 . Those high adsorption energies suggest the formation of Kubas complexes.² The H–H distances (from 0.80 to 0.95 \AA) for $n = 1-3, 7$, and $9-11$ are elongated by 0.05–0.20 \AA compared with the bond length of the free H_2 molecule ($d_{\text{exp}}(\text{H}-\text{H}) = 0.74 \text{\AA}$, $d_{\text{calc}}(\text{H}-\text{H}) = 0.75 \text{\AA}$), indicating an activation of the adsorbed H_2 . For sizes $n = 4-6, 8$, and 12 , the H–H bond lengths (0.75 or 0.76 \AA) are almost the same to that of the free H_2 molecule. The values of $-E_{\text{ads}}(2\text{H})$ are in the range of 0.20 to 1.31 eV. It can be seen that, except for $n = 2$ and 3 , dissociative adsorption of H_2 is thermodynamically favorable over molecular adsorption. Thus, it can be inferred that for $n = 1$ and $4-12$, the H_2 molecule approaching to the bare clusters Al_nRh^+ undergoes a metastable molecular adsorption state to dissociate finally. As is shown in Figure S9 in the SI, the adsorption and dissociation of H_2 on AlRh^+ cluster is barrierless. The H_2 molecule first adsorbs molecularly on the Rh atom and then dissociates with the two H atoms retaining on the Rh atom.

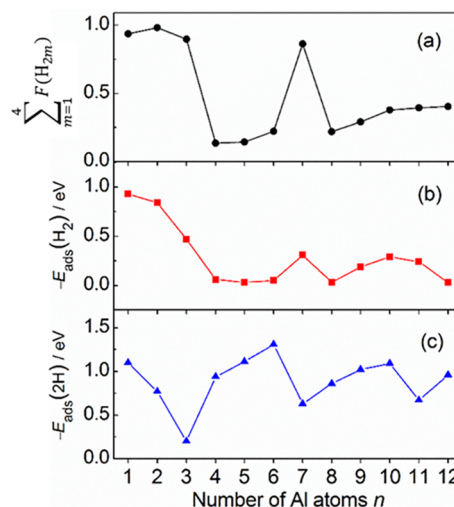


Figure 3. Correlation of the total abundances, $\sum_{m=1}^4 F(\text{H}_{2m})$, of $\text{Al}_n\text{RhH}_{2m}^+$ ($n = 1-12, m = 1-4$) with the calculated molecular, $-E_{\text{ads}}(\text{H}_2)$, and dissociative, $-E_{\text{ads}}(2\text{H})$, adsorption energies.

Figure 3 compares the total abundances, $\sum_{m=1}^4 F(\text{H}_{2m})$, of $\text{Al}_n\text{RhH}_{2m}^+$ ($n = 1-12, m = 1-4$) with the calculated adsorption energies, $-E_{\text{ads}}(\text{H}_2)$ and $-E_{\text{ads}}(2\text{H})$, for single H_2 adsorption on Al_nRh^+ ($n = 1-12$). There is a strong correlation of the calculated $-E_{\text{ads}}(\text{H}_2)$ energies with the experimental fractions, $\sum_{m=1}^4 F(\text{H}_{2m})$, while there is no clear correlation of $\sum_{m=1}^4 F(\text{H}_{2m})$ with the $-E_{\text{ads}}(2\text{H})$ energies. At this point, there are two possible explanations for these correlations: (i) the

molecularly adsorbed state is the experimentally probed configuration or (ii) the formation of the molecularly adsorbed state is the rate-determining step in the adsorption process. As will be discussed in the next section, the IRMPD experiments demonstrate that the first explanation is not correct for most of the probed sizes, so the energetic stability of the molecularly adsorbed state must be the determining factor in the hydrogen adsorption process.

3.4. Comparisons of the IRMPD Spectra with the Calculated IR Spectra.

IRMPD spectra of $\text{Al}_n\text{RhH}_2^+$ ($n = 3-10$) and $\text{Al}_n\text{RhH}_4^+$ ($n = 2$ and 7) are shown in Figure 4

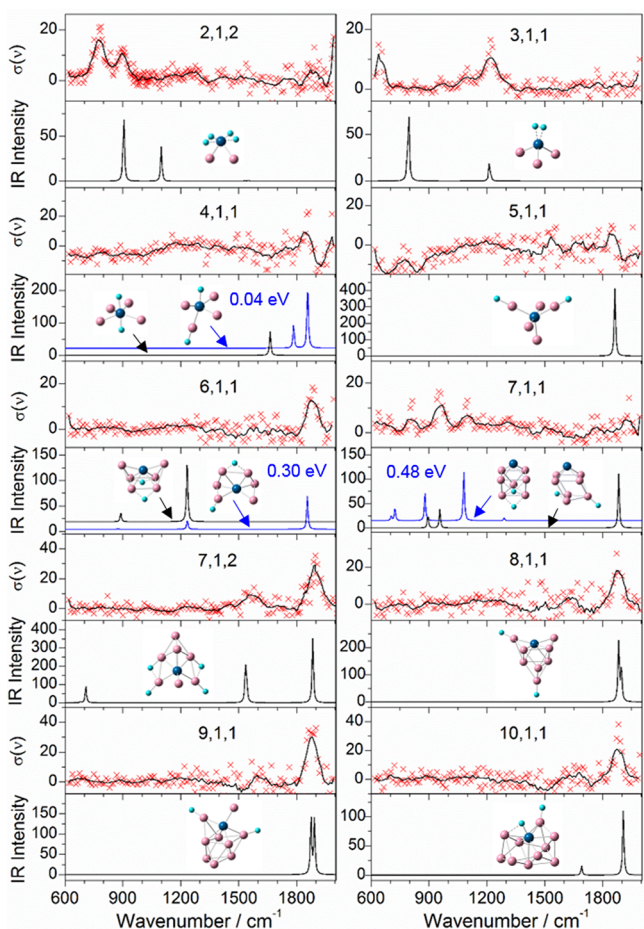


Figure 4. Comparisons of IRMPD spectra (top panels, the crosses are the original data points and the full lines correspond to six-point running averages) of $\text{Al}_2\text{RhH}_4^+$, $\text{Al}_7\text{RhH}_4^+$, and $\text{Al}_n\text{RhH}_2^+$ ($n = 3-10$) with calculated harmonic IR spectra (bottom panels, without scaling) of the lowest energy structures obtained under PBE/Def2TZVP level. For $\text{Al}_n\text{RhH}_2^+$ ($n = 4, 6, \text{ and } 7$), the spectrum of a second isomer is included (blue lines). The labels $n, 1, m$ refer to $\text{Al}_n\text{RhH}_{2m}^+$. The experimental cross section $\sigma(\nu)$ and the calculated IR intensity are given in arbitrary units and $\text{km}\cdot\text{mol}^{-1}$, respectively.

together with the PBE/Def2TZVP calculated unscaled harmonic IR spectra of the lowest-lying isomers. In addition, the IRMPD spectra of $\text{Al}_2\text{RhH}_4^+$ and $\text{Al}_n\text{RhH}_2^+$ ($n = 3-6$) are compared with the calculated anharmonic IR spectra in Table S1 and Figure S10 in the Supporting Information (SI). Comparisons of the IRMPD spectra of AlRhH_{2m}^+ ($m = 3$ and 4), $\text{Al}_n\text{RhH}_4^+$ ($n = 2, 7, 11, \text{ and } 12$), and $\text{Al}_n\text{RhH}_2^+$ ($n = 3-10$ and 12) with the corresponding calculated harmonic IR spectra

for several low-lying isomers of each size are given in Figures S11–S14 in the SI.

Inspection of the calculated vibrational frequencies and the corresponding atomic motion allows one to assign different wavenumber ranges to different hydrogen binding geometries. Most adsorption bands in the $650-900\text{ cm}^{-1}$ range can be assigned to the symmetrical stretching vibrations of $\text{Rh}-\text{H}_2$ bonds. The asymmetrical stretching vibrations of $\text{Rh}-\text{H}_2$ bonds are located around 1200 cm^{-1} . These vibrational frequencies are similar to those observed for molecularly adsorbed hydrogen on transition metal (V, Fe, Co, and Ni) clusters.^{9,34} Bands in the range of $1700-1800\text{ cm}^{-1}$ correspond to the stretching vibrational modes of $\text{Rh}-\text{H}$ bonds and those in the $1850-1900\text{ cm}^{-1}$ range to the stretching modes of $\text{Al}-\text{H}$ bonds, with the H atoms bound terminally to the Al atoms. Other bands in the ranges of $700-800$, $950-1100$, $1540-1600\text{ cm}^{-1}$ can be attributed to H atoms bound at bridging and facet sites formed by Al atoms and correspond to the asymmetrical stretching, rocking, and wagging vibrational modes of $\text{Al}-\text{H}-\text{Al}$ moieties. Observed bands for $\text{Al}-\text{H}$, $\text{Rh}-\text{H}$, and $\text{Al}-\text{H}-\text{Al}$ vibration modes are indications for dissociative H_2 adsorption. Moreover, the $\text{Al}-\text{H}$ and $\text{Al}-\text{H}-\text{Al}$ bonds imply H_2 dissociation and spillover from the Rh dopant to the aluminum framework.

For $\text{Al}_2\text{RhH}_4^+$, two bands at 790 and 910 cm^{-1} are observed, which are assigned, by comparison to the calculated spectrum for the lowest energy isomer, to the symmetric stretching modes of two $\text{Rh}-\text{H}_2$ bonds at 904 and 1099 cm^{-1} . An additional feature at the high end of the wavenumber range, around $1900-2000\text{ cm}^{-1}$, suggests the presence of more than one isomer in the experiment. As mentioned before, bands in this range can be most likely attributed to on-top $\text{H}-\text{Al}$ stretching modes (such as present in isomer 2B; see Figures S3 and S11 in the SI). For $\text{Al}_3\text{RhH}_2^+$, the bands at 650 and 1230 cm^{-1} in the IRMPD spectrum are similarly assigned to the calculated symmetric and asymmetric stretching modes of $\text{Rh}-\text{H}_2$ at 793 and 1214 cm^{-1} . The symmetric stretching mode is blue-shifted by about 140 cm^{-1} while the asymmetric stretching mode is slightly red-shifted. For $\text{Al}_2\text{RhH}_4^+$ and $\text{Al}_3\text{RhH}_2^+$, the calculated symmetrical vibrational modes of $\text{Rh}-\text{H}_2$ are significantly blue-shifted compared to the bands in the IRMPD spectra. This implies that the calculations overestimate the $\text{Rh}-\text{H}_2$ bond strength, which has been observed as well in other studies.^{9,34} Despite the blue-shift, the calculated relative intensities of peaks are in agreement with the experiment, which supports the assignment of the molecular hydrogen binding configurations for these two sizes. The spectra of other isomers (see Figure S11 in the SI) are in less good agreement with the experiment. Bands in the calculated anharmonic IR spectra of $\text{Al}_2\text{RhH}_4^+$ and $\text{Al}_3\text{RhH}_2^+$ (see Figure S10 in the SI) are red-shifted by $40-110\text{ cm}^{-1}$ compared to the harmonic spectrum and thus agree better with the peaks in the IRMPD spectrum.

The low abundances of the hydrogenated complexes in the mass spectra for $n = 4, 5, 6$ result in IRMPD spectra with a lower signal-to-noise ratio. For $\text{Al}_4\text{RhH}_2^+$, the only discernible feature is a band at 1850 cm^{-1} . The calculated harmonic IR spectrum of the lowest energy structure (which has both of the two H atoms bound to Rh) is significantly red-shifted compared to the experimental IRMPD spectra. A better agreement is found for the second low-lying isomer (one of the two H atoms bind to Rh, the other one bind to Al), which is 0.04 eV higher in energy. The low quality of the IRMPD

Table 2. Bands Observed in the IRMPD Spectra and the PBE/Def2TZVP Calculated Harmonic Infrared Active Modes of the Lowest Energy Structures of $\text{Al}_n\text{RhH}_2^+$ ($n = 3-10$) and $\text{Al}_n\text{RhH}_4^+$ ($n = 2$ and 7)^a

$n,1,m$	$\nu(\text{IRMPD})/\text{cm}^{-1}$	$\nu(\text{calcd harmonic})/\text{cm}^{-1}$
2,1,2	790, 910, (2000)	Rh–H ₂ : 904, 1099
3,1,1	650, 1220	Rh–H ₂ : 793, 1214
4,1,1		Rh–H: 1666
4,1,1 (Iso 0.04 eV)	1860	Rh–H: 1785; Al–H: 1858
5,1,1	1860	Al–H: 1849, 1851
6,1,1		Al–H–Al: 889, 1232, 1234
6,1,1 (Iso 0.30 eV)	1880	Al–H–Al: 1229; Al–H: 1851
7,1,1		Al–H–Al: 894, 956; Al–H: 1884
7,1,1 (Iso 0.48 eV)	810, 950, 1100, (1920)	Al–H–Al: 704, 724, 879, 1081
7,1,2	1550, 1890	Al–H–Al: 1535, 1542; Al–H: 1883, 1885
8,1,1	1880	Al–H: 1885, 1901
9,1,1	1890	Al–H: 1879, 1896
10,1,1	1890	Rh–H: 1699; Al–H: 1911

^aA second isomer is given for $\text{Al}_n\text{RhH}_2^+$ ($n = 4, 6,$ and 7). Symbols $n,1,m$ indicate $\text{Al}_n\text{RhH}_{2m}^+$.

spectrum of $\text{Al}_3\text{RhH}_2^+$ renders it difficult to make a definite assignment. However, the harmonic IR spectrum of the calculated lowest energy structure of $\text{Al}_3\text{RhH}_2^+$ has two H–Al stretching modes at 1849 and 1851 cm^{-1} , which seem to correspond to the experimental feature around 1860 cm^{-1} . Notice the negative experimental cross section between 600–800 cm^{-1} , which suggests ingrowth from clusters with more than one hydrogen molecule adsorbed. The abundances of these complexes, however, are so small that barely any depletion bands can be distinguished in their IRMPD spectra. For $\text{Al}_6\text{RhH}_2^+$, the experimental IR spectrum has a single band at 1880 cm^{-1} , whereas the calculated lowest energy structure has two modes at 900 cm^{-1} and 1250 cm^{-1} , corresponding to Al–H–Al bridging bonds. For the second isomer (0.30 eV higher in energy), the calculated Al–H stretching mode agrees well with the intense experimental band centered around 1880 cm^{-1} , but the lower intensity Al–H–Al stretching mode at 1229 cm^{-1} cannot be distinguished in the experiment.

For $\text{Al}_7\text{RhH}_2^+$, there is poor agreement between the IRMPD spectrum and the calculated harmonic IR spectrum of the lowest energy structure, since the Al–H stretching mode around 1900 cm^{-1} is very weak in the IRMPD spectrum (if present at all). Also for other low-lying isomers (relative energy difference within 0.4 eV), there is no agreement (Figure S12). Only one higher energy (0.48 eV) isomer that has one bridging and one facet H atom reproduces the four bands in the range of 700–1100 cm^{-1} in the IRMPD spectrum fairly well. For $\text{Al}_7\text{RhH}_4^+$, the calculated harmonic IR spectrum of the lowest energy structure matches the IRMPD spectrum well. For $\text{Al}_n\text{RhH}_2^+$ ($n = 8-10$), the experimental spectra are characterized by a pronounced band around 1900 cm^{-1} , corresponding to the calculated Al–H stretching modes of the tentative ground-state geometries.

The calculated IR spectra of the lowest energy structures, with exception of $\text{Al}_n\text{RhH}_2^+$ ($n = 4, 6,$ and 7), are in reasonable agreement with the experimental IRMPD spectra. It should be noted that the lowest energy structures of $\text{Al}_n\text{RhH}_{2m}^+$ might not be detected in the experiment due to energy barriers along the reaction pathways. Also, as is shown in Figures S2–S8 in the SI, for most of the $\text{Al}_n\text{RhH}_{2m}^+$ clusters, some isomers with similar H binding modes are close in energy to the ground state structures. The calculated IR spectra of those low-lying energy isomers are very similar to that of the ground state structures in the probed spectral range (Figures S11–S14 in

the SI). These comparisons illustrate that it may be difficult to unambiguously assign the geometric structures of the hydrogenated clusters based on the available experimental data. However, one can be more confident about the hydrogen-binding configuration (molecular or dissociative, transfer away or retaining at the doped Rh active center). Examples are the fingerprint signals for molecular H₂ binding to Al_2Rh^+ and Al_3Rh^+ and for dissociative hydrogen adsorption in bridging or atop configurations for other sizes.

Table 2 summarizes the observed features in the IRMPD spectra for $\text{Al}_n\text{RhH}_2^+$ ($n = 3-10$) and $\text{Al}_n\text{RhH}_4^+$ ($n = 2$ and 7) that match with the calculated harmonic IR band positions of the identified isomers. Bands that are found in the experiment but do not show up in the calculated spectra of the assigned isomer are given in brackets.

4. DISCUSSION

The size-specific geometric and electronic structures of small metal clusters cause a dramatic size-dependent reactivity for H₂ chemisorption.^{35–39} In earlier studies, correlations were found between the reactivity and the ionization potentials or electron affinities of the clusters, which can be explained by a charge-transfer model.^{35,36} In this work, the reactivity of the Al_nRh^+ clusters toward H₂ is found to be strongly size-dependent, with $n = 1-3$ and 7 being the most reactive sizes. The initial molecular adsorption of H₂ is identified as the rate-determining step for hydrogen interaction, since the calculated molecular H₂ adsorption energies correlate well with the total mass abundance fractions of the hydrogenated clusters. Similar molecular H₂ adsorption precursor states have been observed in reactions of transition metal clusters M_n ($M = \text{Fe}, \text{Co}, \text{Ni},$ and W) with H₂/D₂.³⁹ Such precursor states essentially give the H₂ molecule more time to probe the potential energy surfaces for possible dissociation channels. To interpret the size-dependent reactivity of Al_nRh^+ toward H₂, several factors that may contribute to the stability and selectivity of H₂ adsorption are considered, including the geometric structures, charge distributions, ionization energies, and electron affinities of the bare clusters Al_nRh^+ , as well as charge transfer between the H₂ molecule and the Al_nRh^+ clusters.

4.1. Geometric Effects. As the number of Al atoms (n) in Al_nRh^+ increases, the preferred position of the Rh atom gradually moves from top sites to convex capped sites and partially encapsulated sites surrounded by aluminum cage

Table 3. PBE/Def2TZVP Calculated NPA Charges in Al_nRh^+ , $\text{Al}_n\text{Rh}\cdot\text{H}_2^+$, and $\text{Al}_n\text{RhH}_2^+$ ($n = 1-12$) as well as the Vertical Electron Affinity (E_{VEA}) and Ionization Energy (E_{VIE}) of $\text{Al}_n\text{Rh}^{+\text{a}}$

n	$q(\text{Rh})/e$	$E_{\text{VIE}}/e\text{V}$	$E_{\text{VEA}}/e\text{V}$	$q(\text{Rh})-\text{H}_2/e$	$q(\text{Rh})-2\text{H}/e$	$q(\text{H}_2)/e$	$q(2\text{H})/e$
1	0.18	17.07	6.76	-0.13	-0.33	0.17	0.22
2	-0.72	12.88	6.38	-1.01	-0.81	0.14	-0.31
3	-1.61	11.16	6.31	-2.14	-1.58	0.22	-0.46
4	-2.33	10.91	5.50	-2.43	-3.35	0.04	0.04
5	-3.91	9.73	5.37	-3.91	-4.01	0.01	-0.78
6	-3.30	10.19	5.67	-3.32	-2.70	0.03	-0.76
7	-1.23	10.55	6.30	-1.68	-1.29	0.20	-0.66
8	-2.37	10.05	5.30	-2.35	-2.55	0.04	-0.61
9	-2.99	9.73	5.90	-2.36	-2.97	0.29	-0.65
10	-2.49	9.76	5.74	-2.54	-2.68	0.31	-0.26
11	-2.37	9.66	5.98	-2.75	-2.97	0.34	-0.61
12	-2.62	9.38	5.48	-2.60	-3.18	0.04	-0.17

^aThe symbols $q(\text{Rh})$, $q(\text{Rh})-\text{H}_2$, and $q(\text{Rh})-2\text{H}$ represent charges on the Rh atom in Al_nRh^+ , $\text{Al}_n\text{Rh}\cdot\text{H}_2^+$, and $\text{Al}_n\text{RhH}_2^+$, respectively. The symbols $q(\text{H}_2)$ and $q(2\text{H})$ indicate charges on hydrogen in $\text{Al}_n\text{Rh}\cdot\text{H}_2^+$ and $\text{Al}_n\text{RhH}_2^+$.

frameworks. Calculations indicate that the preferred binding site for molecular H_2 adsorption is the Rh atom and H_2 always binds to the Rh atom when it is available. The Rh atom in Al_nRh^+ ($n = 1-3$ and 7) is less coordinated and easily accessible for H_2 adsorption. For $n = 4$ and 9–11, the Rh coordination number increases and Rh becomes shielded, which is unfavorable for H_2 adsorption. For $n = 5, 6, 8,$ and 12, besides high coordination of the Rh atom, the Rh atom is partially encapsulated by aluminum atoms, thereby impeding H_2 adsorption. For those clusters, it is energetically more favorable for the H_2 molecule to adsorb on an Al atom. In light of the inertness of the majority of aluminum clusters toward H_2 , this is quite remarkable. Thus, the location of the Rh dopant (top sites with lower coordination or inside positions with higher coordination) has a great influence on the region-selectivity involved in H_2 molecular adsorption. Note that the structures of the Al_nRh^+ ($n = 1-12$) clusters do not change noticeably upon molecular H_2 adsorption, but do for dissociative adsorption, especially for the larger sizes ($n = 7-12$).

4.2. Charge Distribution and Transfer. Table 3 summarizes the natural population analysis (NPA) charge distributions for Al_nRh^+ , $\text{Al}_n\text{Rh}\cdot\text{H}_2^+$, and $\text{Al}_n\text{RhH}_2^+$ ($n = 1-12$) as well as the vertical electron affinity (E_{VEA}) and ionization energy (E_{VIE}) of Al_nRh^+ . Figure 5 compares the total abundances of $\text{Al}_n\text{RhH}_{2m}^+$, $\sum_{m=1}^4 F(\text{H}_{2m})$, with the NPA charges on the Rh atom ($q(\text{Rh})/e$) as well as the E_{VEA} and E_{VIE} of Al_nRh^+ clusters. The $\sum_{m=1}^4 F(\text{H}_{2m})$ correlates well with $q(\text{Rh})$. This may indicate that the charge on Rh plays an important role in the interactions of Al_nRh^+ with H_2 . In Figure 6, electron density difference maps are plotted for H_2 molecular adsorption on Al_nRh^+ ($n = 1-12$). For Al_nRh^+ ($n = 1-3, 7,$ and 9–11), on which the H_2 molecule adsorbs on the Rh dopant atom, complex formation leads to an increase of the electron density in the region between the clusters and the H_2 molecule and it decreases on both the clusters (specifically the Rh atom) and the H_2 molecule. This is representative for the formation of a covalent bond. For the other sizes ($n = 4-6, 8,$ and 12), there is no significant charge transfer between the clusters (Rh or Al centers) and the H_2 molecule.

4.3. Influences of the Electron Affinities and Ionization Energies. The electron affinity and ionization energy directly reflect variations of the valence electron

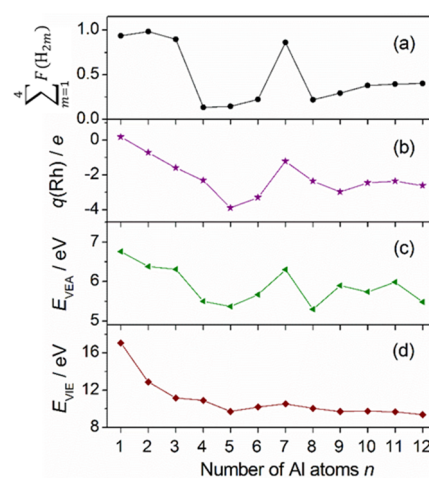


Figure 5. Correlations of the total abundances of $\text{Al}_n\text{RhH}_{2m}^+$ ($n = 1-12$, $m = 1-4$), $\sum_{m=1}^4 F(\text{H}_{2m})$, with the NPA charges on the Rh atom in Al_nRh^+ , $q(\text{Rh})$, as well as with the vertical electron affinity, E_{VEA} , and vertical ionization energy, E_{VIE} , of Al_nRh^+ clusters.

energies, which can determine the size-dependent reactivity of metal clusters. There is a strong correlation between the total abundances of $\text{Al}_n\text{RhH}_{2m}^+$, $\sum_{m=1}^4 F(\text{H}_{2m})$, with the calculated vertical electron affinities, E_{VEA} , of Al_nRh^+ clusters. No clear correlation is found for the calculated vertical ionization energies, E_{VIE} . The calculated E_{VIE} for Al_nRh^+ clusters generally decrease with cluster size growing from 1 to 12. The higher E_{VEA} and E_{VIE} values for the smallest clusters Al_nRh^+ ($n = 1-3$) may indicate that higher electron affinities and ionization energies contribute to molecular H_2 adsorption. Similarly, in the experimental investigation of hydrogen chemisorption on anionic titanium clusters, it was concluded that molecular H_2 adsorption is favored over dissociative adsorption due to the higher ionization energies of smaller clusters.³⁸

5. CONCLUSION

The gas-phase interaction of H_2 with singly rhodium doped aluminum clusters Al_nRh^+ ($n = 1-12$) is investigated by a combination of mass spectrometry, IRMPD spectroscopy, and DFT calculations. A strongly size-dependent reactivity of Al_nRh^+ clusters toward H_2 is observed experimentally. DFT

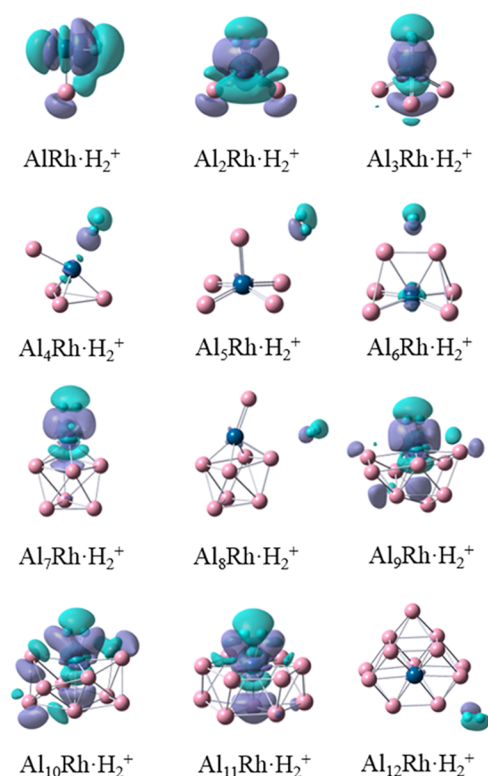


Figure 6. Electron density difference maps for molecular H_2 adsorption on Al_nRh^+ ($n = 1-12$) clusters. The violet and cyan isosurfaces (+0.001 and -0.001 au, respectively) represent the region in which electron density is increased and decreased after formation of the complex, respectively.

calculations indicate that several factors, including the geometric structures, the charge on the Rh dopant atom, the electron affinities, and ionization energies of the bare clusters Al_nRh^+ , as well as the charge transfer between Al_nRh^+ clusters and the H_2 molecule, are responsible for this distinct size-dependent reactivity. It is thermodynamically favorable for H_2 to adsorb molecularly on Al_2Rh^+ and Al_3Rh^+ , while dissociative adsorption is preferred for other sizes ($n = 1$ and $4-12$). For Al_nRh^+ ($n = 1-3, 7$, and $9-11$), the H_2 molecule adsorbs on the Rh dopant atom and electron density shifts from the clusters and the H_2 molecule toward the region between them to form a covalent bond. For other sizes ($n = 4-6, 8$, and 12), on the other hand, there is no significant charge transfer between the clusters and the H_2 molecule to facilitate the interaction. Although the clusters investigated in this work are much smaller than the bulk materials that are of interest for hydrogen storage, our results give insight at the molecular level into the hydrogen adsorption and dissociation on transition metal doped aluminum-based materials, key elementary reaction steps in the hydrogenation of these storage media.

■ ASSOCIATED CONTENT

📄 Supporting Information

The Supporting Information is available free of charge on the ACS Publications website at DOI: 10.1021/acs.jpcc.8b04332.

PBE/SDD&TZVP calculated low-lying energy isomers for Al_nRh^+ ($n = 1-12$), $Al_nRhH_{2m}^+$ ($n = 1-3, m = 1-4$), and $Al_nRhH_{2m}^+$ ($n = 4-12, m = 1-2$); calculated reaction pathway for H_2 adsorption and dissociation on $AlRh^+$; comparison of IRMPD spectra for $Al_2RhH_4^+$ and

$Al_nRhH_2^+$ ($n = 3-6$) with computed anharmonic IR spectra; and comparisons of the IRMPD spectra for $AlRhH_{2m}^+$ ($m = 3$ and 4), $Al_nRhH_4^+$ ($n = 2, 7, 11$, and 12), and $Al_nRhH_2^+$ ($n = 3-10$ and 12) with the PBE/SDD&TZVP calculated harmonic IR spectra for low-lying isomers (PDF)

■ AUTHOR INFORMATION

Corresponding Author

*E-mail: ewald.janssens@kuleuven.be. Tel.: +32 16 32 72 07.

ORCID

Wieland Schöllkopf: 0000-0003-0564-203X

Minh Tho Nguyen: 0000-0002-3803-0569

André Fielicke: 0000-0003-0400-0932

Ewald Janssens: 0000-0002-5945-1194

Notes

The authors declare no competing financial interest.

■ ACKNOWLEDGMENTS

This work is supported by the KU Leuven Research Council (GOA/14/007) and by the Research Foundation Flanders (FWO, Project G.0B411.5N). J.V. and P.F. thank the FWO for a PhD fellowship and a postdoctoral fellowship, respectively. E.M.F. thanks the RyC contract (ref. RYC-2014-15261) of the Spanish Minister of Economy, Industry and Competitiveness. A.F. thanks the Deutsche Forschungsgemeinschaft for a Heisenberg grant (FI893/5).

■ REFERENCES

- Schlapbach, L.; Züttel, A. Hydrogen-Storage Materials for Mobile Applications. *Nature* **2001**, *414*, 353–358.
- Kubas, G. J. Fundamentals of H_2 Binding and Reactivity on Transition Metals Underlying Hydrogenase Function and H_2 Production and Storage. *Chem. Rev.* **2007**, *107*, 4152–4205.
- Niaz, S.; Manzoor, T.; Pandith, A. H. Hydrogen Storage: Materials, Methods and Perspectives. *Renewable Sustainable Energy Rev.* **2015**, *50*, 457–469.
- van den Berg, A. W. C.; Areán, C. O. Materials for Hydrogen Storage: Current Research Trends and Perspectives. *Chem. Commun.* **2008**, 668–681.
- Sakintuna, B.; Lamari-Darkrim, F.; Hirscher, M. Metal Hydride Materials for Solid Hydrogen Storage: A Review. *Int. J. Hydrogen Energy* **2007**, *32*, 1121–1140.
- Orimo, S.-i.; Nakamori, Y.; Eliseo, J. R.; Züttel, A.; Jensen, C. M. Complex Hydrides for Hydrogen Storage. *Chem. Rev.* **2007**, *107*, 4111–4132.
- Schüth, F.; Bogdanović, B.; Felderhoff, M. Light Metal Hydrides and Complex Hydrides for Hydrogen Storage. *Chem. Commun.* **2004**, 2249–2258.
- Lang, S. M.; Bernhardt, T. M. Gas Phase Metal Cluster Model Systems for Heterogeneous Catalysis. *Phys. Chem. Chem. Phys.* **2012**, *14*, 9255–9269.
- Swart, I.; de Groot, F. M. F.; Weckhuysen, B. M.; Gruene, P.; Meijer, G.; Fielicke, A. H_2 Adsorption on 3d Transition Metal Clusters: A Combined Infrared Spectroscopy and Density Functional Study. *J. Phys. Chem. A* **2008**, *112*, 1139–1149.
- Pino, I.; Kroes, G. J.; van Hemert, M. C. Hydrogen Dissociation on Small Aluminum Clusters. *J. Chem. Phys.* **2010**, *133*, 184304.
- Nonose, S.; Sone, Y.; Onodera, K.; Sudo, S.; Kaya, K. Reactivity Study of Alloy Clusters Made of Aluminum and Some Transition-Metals with Hydrogen. *Chem. Phys. Lett.* **1989**, *164*, 427–432.
- Henry, D. J.; Yarovsky, I. Dissociative Adsorption of Hydrogen Molecule on Aluminum Clusters: Effect of Charge and Doping. *J. Phys. Chem. A* **2009**, *113*, 2565–2571.

- (13) Wang, L.; Zhao, J.; Zhou, Z.; Zhang, S. B.; Chen, Z. First-Principles Study of Molecular Hydrogen Dissociation on Doped $Al_{12}X$ ($X = B, Al, C, Si, P, Mg, \text{ and } Ca$) Clusters. *J. Comput. Chem.* **2009**, *30*, 2509–14.
- (14) Charkin, O. P.; Mikhailin, A. A.; Klimenko, N. M. Theoretical Modeling of Elementary Reactions of Dissociative Addition of an H_2 Molecule to Aluminum Clusters MAl_{12} Doped with Early $3d$ and $4d$ Transition Metal Atoms. *Russ. J. Inorg. Chem.* **2013**, *58*, 1479–1488.
- (15) Guo, L. First-Principles Study of Molecular Hydrogen Adsorption and Dissociation on Al_nCr ($n = 1-13$) Clusters. *J. Phys. Chem. A* **2013**, *117*, 3458–3466.
- (16) Duš, R.; Nowicka, E.; Nowakowski, R. Hydrogen Adsorption on Rhodium: Hydride Formed on the Surface of Thin Rhodium Films. *Appl. Surf. Sci.* **2008**, *254*, 4286–4291.
- (17) Jung, S. C.; Kang, M. H. Effect of Hydrogen on the Surface Relaxation of Pd(100), Rh(100), and Ag(100). *Phys. Rev. B: Condens. Matter Mater. Phys.* **2005**, *72*, 205419.
- (18) Wang, X.; Andrews, L. Infrared Spectra of Rhodium Hydrides in Solid Argon, Neon, and Deuterium with Supporting Density Functional Calculations. *J. Phys. Chem. A* **2002**, *106*, 3706–3713.
- (19) Trivedi, R.; Bandyopadhyay, D. Study of Adsorption and Dissociation Pathway of H_2 Molecule on Mg_nRh ($n = 1-10$) Clusters: A First Principle Investigation. *Int. J. Hydrogen Energy* **2016**, *41*, 20113–20121.
- (20) Vanbuel, J.; Fernández, E. M.; Ferrari, P.; Gewinner, S.; Schöllkopf, W.; Balbás, L. C.; Fielicke, A.; Janssens, E. Hydrogen Chemisorption on Singly Vanadium-Doped Aluminum Clusters. *Chem. - Eur. J.* **2017**, *23*, 15638–15643.
- (21) Vanbuel, J.; Jia, M.-y.; Ferrari, P.; Gewinner, S.; Schöllkopf, W.; Nguyen, M. T.; Fielicke, A.; Janssens, E. Competitive Molecular and Dissociative Hydrogen Chemisorption on Size Selected Doubly Rhodium Doped Aluminum Clusters. *Top. Catal.* **2018**, *61*, 62–70.
- (22) Truong, N. X.; Haertelt, M.; Jaeger, B. K. A.; Gewinner, S.; Schöllkopf, W.; Fielicke, A.; Dopfer, O. Characterization of Neutral Boron-Silicon Clusters Using Infrared Spectroscopy: The Case of Si_4B . *Int. J. Mass Spectrom.* **2016**, *395*, 1–6.
- (23) Schöllkopf, W.; Gewinner, S.; Junkes, H.; Paarmann, A.; von Helden, G.; Bluem, H.; Todd, A. M. M.; Biedron, S. G. The new IR and THz FEL Facility at the Fritz Haber Institute in Berlin. *Proc. SPIE* **2015**, *9512*, 95121L.
- (24) Nesbitt, D. J.; Field, R. W. Vibrational Energy Flow in Highly Excited Molecules: Role of Intramolecular Vibrational Redistribution. *J. Phys. Chem.* **1996**, *100*, 12735–12756.
- (25) Frisch, M. J.; Trucks, G. W.; Schlegel, H. B.; Scuseria, G. E.; Robb, M. A.; Cheeseman, J. R.; Scalmani, G.; Barone, V.; Mennucci, B.; Petersson, G. A., et al. *Gaussian 09*, revision E.1; Gaussian, Inc.: Wallingford, CT, 2013.
- (26) Perdew, J. P.; Burke, K.; Ernzerhof, M. Generalized Gradient Approximation Made Simple. *Phys. Rev. Lett.* **1996**, *77*, 3865–3868.
- (27) Petrie, S.; Stranger, R. DFT and Metal-Metal Bonding: A Dys-Functional Treatment for Multiply Charged Complexes? *Inorg. Chem.* **2004**, *43*, 2597–2610.
- (28) Romo-Ávila, S. L.; Guirado-López, R. A. Adsorption of Nitric Oxide on Small Rh_n^{\pm} Clusters: Role of the Local Atomic Environment on the Dissociation of the N-O Bond. *J. Phys. Chem. A* **2012**, *116*, 1059–68.
- (29) Wang, Y.; Lv, J.; Zhu, L.; Ma, Y. Crystal Structure Prediction Via Particle-Swarm Optimization. *Phys. Rev. B: Condens. Matter Mater. Phys.* **2010**, *82*, 094116.
- (30) Lv, J.; Wang, Y.; Zhu, L.; Ma, Y. Particle-Swarm Structure Prediction on Clusters. *J. Chem. Phys.* **2012**, *137*, 084104.
- (31) Igel-Mann, G.; Stoll, H.; Preuss, H. Pseudopotentials for Main Group Elements (IIIa through VIIa). *Mol. Phys.* **1988**, *65*, 1321–1328.
- (32) Schäfer, A.; Huber, C.; Ahlrichs, R. Fully Optimized Contracted Gaussian Basis Sets of Triple Zeta Valence Quality for Atoms Li to Kr. *J. Chem. Phys.* **1994**, *100*, 5829–5835.
- (33) Weigend, F.; Ahlrichs, R. Balanced Basis Sets of Split Valence, Triple Zeta Valence and Quadruple Zeta Valence Quality for H to Rn: Design and Assessment of Accuracy. *Phys. Chem. Chem. Phys.* **2005**, *7*, 3297–3305.
- (34) Swart, I.; Gruene, P.; Fielicke, A.; Meijer, G.; Weckhuysen, B. M.; de Groot, F. M. F. Molecular Adsorption of H_2 on Small Cationic Nickel Clusters. *Phys. Chem. Chem. Phys.* **2008**, *10*, 5743–5745.
- (35) Conceicao, J.; Laaksonen, R. T.; Wang, L. S.; Guo, T.; Nordlander, P.; Smalley, R. E. Photoelectron Spectroscopy of Transition-Metal Clusters: Correlation of Valence Electronic Structure to Reactivity. *Phys. Rev. B: Condens. Matter Mater. Phys.* **1995**, *51*, 4668–4671.
- (36) Whetten, R. L.; Cox, D. M.; Trevor, D. J.; Kaldor, A. Correspondence between Electron Binding Energy and Chemisorption Reactivity of Iron Clusters. *Phys. Rev. Lett.* **1985**, *54*, 1494–1497.
- (37) Elkind, J. L.; Weiss, F. D.; Alford, J. M.; Laaksonen, R. T.; Smalley, R. E. Fourier Transform Ion Cyclotron Resonance Studies of H_2 Chemisorption on Niobium Cluster Cations. *J. Chem. Phys.* **1988**, *88*, 5215–5224.
- (38) Burkart, S.; Blessing, N.; Ganteför, G. Indication of a Size-Dependent Transition from Molecular to Dissociative Chemisorption on Clusters. *Phys. Rev. B: Condens. Matter Mater. Phys.* **1999**, *60*, 15639–15642.
- (39) Knickelbein, M. B. Reactions of Transition Metal Clusters with Small Molecules. *Annu. Rev. Phys. Chem.* **1999**, *50*, 79–115.